THE JOURNAL OF PHYSICAL CHEMISTRY C
A JOURNAL OF THE AMERICAN CHEMICAL SOCIETY

pubs.acs.org/JPCC

Article

Elucidating the Location of Cd^{2+} in Post-synthetically Treated InP Quantum Dots Using Dynamic Nuclear Polarization ^{31}P and ^{113}Cd Solid-State NMR Spectroscopy

Michael P. Hanrahan, Jennifer L. Stein, Nayon Park, Brandi M. Cossairt,* and Aaron J. Rossini*

Cite This: *J. Phys. Chem. C* 2021, 125, 2956−2965

Read Online

ACCESS | Metrics & More | Article Recommendations | Supporting Information

ABSTRACT: Indium phosphide quantum dots (InP QD) are a promising alternative to traditional QD materials that contain toxic heavy elements such as lead and cadmium. However, InP QD obtained from colloidal synthesis are often plagued by poor photoluminescence quantum yields (PL-QYs). In order to improve the PL-QY of InP QD, a number of post-synthetic treatments have been devised. Recently, it has been shown that InP post-synthetically treated with Lewis acid metal divalent cations (M-InP) exhibit enhanced PL-QY; however, the molecular structure and mechanism behind the improved PL-QY are not fully understood. To determine the surface structure of M-InP QD, dynamic nuclear polarization surface-enhanced nuclear magnetic resonance spectroscopy (DNP SENS) experiments were employed on a series of InP magic size clusters treated with Cd ions, InP QD, cadmium phosphide (Cd_3P_2) QD, and Cd-treated InP QD (Cd−InP QD). With the use of DNP SENS, we were able to obtain the 1D ^{31}P and ^{113}Cd NMR spectra, $^{113}Cd\{^{31}P\}$ rotational-echo double-resonance (REDOR) NMR spectra, and $^{31}P\{^{113}Cd\}$ dipolar heteronuclear multiple quantum correlation (D-HMQC) sequence. Changes in the phosphide ^{31}P chemical shifts after Cd treatment provide indirect evidence that some Cd alloys into the sub-surface regions of the particle. DNP-enhanced ^{113}Cd solid-state NMR spectra suggest that most Cd ions are coordinated by oxygen atoms from either carboxylate ligands or surface phosphate groups. $^{113}Cd\{^{31}P\}$ REDOR and $^{31}P\{^{113}Cd\}$ D-HMQC experiments confirm that a subset of Cd ions are located on the surface of Cd−InP QD and coordinated with phosphate groups.

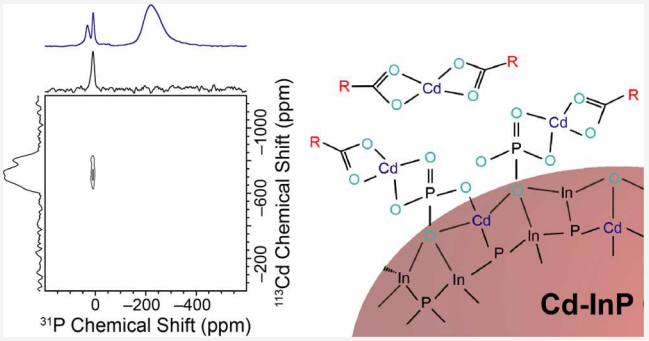

INTRODUCTION

Chalcogen-based semiconductor quantum dots (QD) have many potential technological applications.[1] However, many of the most promising QD materials contain toxic heavy metals (e.g., PbSe, PbS, CdS, CdSe, CdTe, $CsPbBr_3$, and so forth). To limit the environmental effect of these materials, alternative QD free of heavy metals are needed.[2] Indium phosphide (InP) QD are a promising alternative to traditional QD; however, InP QD are often hindered by broad particle size distributions,[3,4] causing emission and absorption in a broad range of wavelengths, and poor photoluminescence quantum yields (PL-QYs).[5] Researchers have developed alternative synthetic routes that use InP magic size clusters (MSC) or molecular compounds as precursors to prepare InP QD with a uniform particle size.[6,7] The PL-QY of InP QD has been improved by fabricating core/shell InP/ZnS,Se QD.[8,9] Alternatively, Stein and co-workers demonstrated that post-synthetic treatment of InP QD with Lewis acid divalent metal cations (Zn^{2+} or Cd^{2+}) can increase the PL-QY to 50%.[10] An extended X-ray absorption fine structure (EXAFS) study of Cd demonstrated Cd−O and Cd−P bonding in the cadmium-treated InP QD (denoted Cd−InP QD).[10] Treatment of Cd−InP with a Lewis base demonstrated removal of Cd ions and a loss of PL-QY.[10] Therefore, this study concluded that divalent metal cations can replace In^{3+} at the surface of the InP QD and/or bind to under-coordinated surface P atoms, eliminating localized QD LUMO states and resulting in improved PL-QY.[10] However, the exact location of the M^{2+} cations and the molecular mechanism underlying the improvements in PL-QY remain unknown. From an environmental standpoint, Zn-treated InP QD would be preferred due to the negligible toxicity of Zn; however, Cd−InP QD showed larger gains in PL-QY.[10] Cd−InP QD are investigated here as they are amenable to study by ^{113}Cd solid-state nuclear magnetic resonance (NMR) spectroscopy.

Solution and solid-state ^{31}P NMR spectroscopy have been previously employed to obtain valuable structural information

Received: October 23, 2020
Revised: January 12, 2021
Published: January 27, 2021

https://dx.doi.org/10.1021/acs.jpcc.0c09601
J. Phys. Chem. C 2021, 125, 2956−2965

about the bulk and surface structure of InP QD and InP MSC.[11−15] In particular, solution ^{31}P NMR has shown that Cd^{2+} cations can be readily substituted into the In positions of InP MSC.[14] While solution ^{31}P NMR works well for probing the phosphorus local environment in MSC and small nanoparticles, larger particles with diameters above several nm possess slow correlation times that are longer than the inverse of the Larmor frequency, resulting in broad NMR signals because of efficient homogeneous transverse relaxation (T_2'). Therefore, larger QD are often more easily studied by solid-state NMR spectroscopy. Unfortunately, previous ^{31}P NMR experiments on InP QD required large sample volumes and/or long experiment times. For example, Pines and co-workers reported ^{1}H → ^{31}P cross-polarization magic angle spinning (CPMAS) experimental times of 10−15 h for InP QD using a 4 mm outer diameter rotor,[11] which typically requires at least 100 mg of sample. Previously, we obtained quantitative ^{31}P direct excitation solid-state NMR spectra of various InP QD with 50 kHz MAS frequency and 1.3 mm rotors (ca. 4 mg of sample). However, between 22 and 124 h of signal averaging was required to obtain 1D ^{31}P solid-state NMR spectra.[16]

Recently, dynamic nuclear polarization (DNP)[17,18] has been used to obtain order of magnitude enhancements in NMR sensitivity for a variety of materials, including QD. In a DNP experiment, the larger polarization of unpaired electron spins is transferred to nuclear spins, typically at cryogenic temperatures. The unpaired electron spins are introduced via the addition of an exogeneous radical polarizing agent (PA). To induce DNP, the sample is then irradiated with high-power microwaves at a specific electron paramagnetic resonance frequency. The sensitivity of solid-state NMR experiments on QD and other nanomaterials can be improved by DNP surface-enhanced NMR spectroscopy (SENS).[19−29] To prepare QD samples for a DNP SENS experiment, a colloidal solution of QD is dispersed on a support material, either mesoporous silica[24] or hexagonal boron nitride (*h*-BN),[27] and then a PA solution is added. Alternatively, to further increase NMR sensitivity, the QD can be precipitated from solution, physically mixed with *h*-BN, and then impregnated with a minimal volume of PA solution.[27]

To elucidate the location of Cd^{2+} in Cd−InP QD, we employed DNP SENS to obtain ^{31}P and ^{113}Cd solid-state NMR spectra of InP MSC treated with various amounts of Cd, 3 nm diameter InP QD with and without Cd treatment, and Cd_3P_2 QD. These samples were prepared for DNP using a recently modified sample preparation procedure where the QD and MSC are dispersed on or physically mixed with *h*-BN.[27] 1D ^{31}P and ^{113}Cd solid-state NMR spectra and ^{31}P−^{113}Cd rotational-echo double resonance (REDOR) and ^{31}P{^{113}Cd} dipolar heteronuclear multiple quantum coherence (D-HMQC) experiments were employed to identify the location of Cd atoms in the post-synthetically treated Cd−InP QD.

RESULTS AND DISCUSSION

We began our investigation by acquiring DNP-enhanced ^{31}P CPMAS solid-state NMR spectra of InP QD and InP MSC with and without post-synthetic treatment with cadmium oleate ($Cd(OA)_2$) (Figure 1). Cd treatment was performed by stirring InP MSC with cadmium oleate in toluene for 20−72 h or by heating a 1-octadecene solution of as-synthesized InP QD with cadmium oleate for 2 h at 200 °C. Samples treated with $Cd(OA)_2$ are denoted Cd−InP QD and Cd−InP MSC,

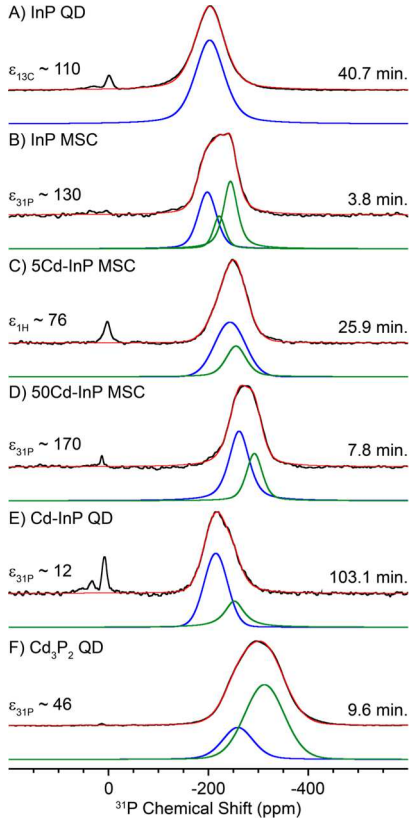

Figure 1. DNP-enhanced ^{1}H → ^{31}P CPMAS spin-echo solid-state NMR spectra of (A) InP QD, (B) InP MSC, (C) 5Cd−InP MSC, (D) 50Cd−InP MSC, (E) Cd−InP QD, and (F) Cd_3P_2 QD. The red spectra are the sum of peak fits, the blue peaks are ^{31}P signals associated with the core/subsurface, and the green peaks are ^{31}P signals associated with the surface or Cd doped to the subsurface. Total experiment times are indicated next to each spectrum. Spectra (A−D) were obtained by impregnating *h*-BN with the MSC or QD TCE solution and a TEKPol TCE solution. Spectra (E,F) were obtained by mixing precipitated QD and *h*-BN, followed by impregnation with a TEKPol TCE solution. Sample DNP enhancements (ε) measured by ^{31}P or ^{13}C CPMAS or ^{1}H direct excitation are noted on the left of each ^{31}P CPMAS spectrum and the total experiment time is indicated on the right.

and the number in front of the sample name indicates the equivalents of Cd to In used during the treatment. Following Cd treatment, the samples were purified by repeated precipitation, washing, and gel permeation chromatography (see the Experimental Section). Importantly, the number of equivalents of Cd used in the treatment does not directly translate into the concentration in the final samples, especially at high equivalents (>20). The final Cd/In ratios were estimated to be 0.35:1 and 2:1 in 5Cd−InP MSC and 50Cd−InP MSC, respectively, as measured by inductively coupled plasma optical emission spectroscopy (ICP-OES). For Cd−InP QD, the final Cd/In ratio was determined to be 0.8:1.

Two different groups of NMR signals are observed in the DNP-enhanced ^{31}P CPMAS solid-state NMR spectra of InP QD and InP MSC. The first set of ^{31}P NMR signals resonates between 0 to 50 ppm. These chemical shifts correspond to phosphate species that are located on the surface of the QD. The phosphates originate from partial oxidation of the QD or MSC.[12,16] Partial oxidation is primarily observed in QD and MSC that have been post-synthetically treated with $Cd(OA)_2$.

https://dx.doi.org/10.1021/acs.jpcc.0c09601
J. Phys. Chem. C 2021, 125, 2956−2965

This observation is consistent with prior studies of InP surface oxidation by ^{31}P solid-state NMR and X-ray fluorescence spectroscopy, which established that carboxylate ligands present during QD synthesis and post-synthetic treatment can cause surface oxidation.[16] A comparison of the ^{31}P CPMAS NMR spectra of Cd−InP QD handled under air-free and ambient conditions show similar relative quantities of the phosphate signal and phosphide NMR signals, confirming that the oxidation primarily occurs during the post-synthetic Cd treatment, rather than during the preparation of samples for DNP NMR experiments (Figure S1).

The second set of ^{31}P NMR signals are very broad ^{31}P peaks with isotropic chemical shifts ranging from −170 to −350 ppm that are attributed to surface and core phosphides, consistent with prior studies of phosphide QD.[11−13,16] The inhomogeneous broadening of the NMR signals arises because the surface, sub-surface, and core phosphides will all have slightly different chemical shifts.[12,30] To confirm which part of the broad phosphide NMR signal is attributed to the core of the QD, a ^{31}P spin diffusion experiment[27,31] was performed on InP QD, 50Cd−InP MSC and Cd−InP QD (Figures S2−S4). The ^{31}P spin diffusion experiment revealed that isotropic ^{31}P chemical shifts of core phosphides are centered at approximately −200 ppm in both InP QD and Cd−InP QD. The ^{31}P chemical shift of microcrystalline InP has previously been reported to be −145 ppm.[11,32] The difference in the ^{31}P chemical shift of microcrystalline InP and InP QD likely arises because quantum confinement effects cause smaller particles to have a larger band gap, resulting in increased nuclear shielding and a more negative chemical shift.[11,30,33−35] Similar relationships between the particle size and chemical shift have been observed in many different QD systems.[11,30,33−35]

The phosphide region of the Cd−InP QD and MSC was fit to two Gaussian/Lorentzian peaks that correspond to NMR signals associated with the core/sub-surface and surface regions of the QD (with the exception of InP MSC which required a three-peak fit. Figure 1 and Table S1). The ^{31}P chemical shifts of the surface and sub-surface phosphides of the MSC shift to more negative values as more equivalents of $Cd(OA)_2$ are used during treatment. A similar observation is made when comparing the phosphide ^{31}P NMR signals of InP QD and Cd_3P_2 QD, where the ^{31}P NMR signals of Cd_3P_2 resonate at a 90 ppm more negative ^{31}P chemical shift (Figure S5). Therefore, these comparisons suggest that phosphides bonded to cadmium will resonate at a lower chemical shift than phosphides bonded to indium.

A comparison of the ^{31}P NMR spectra of InP QD and Cd−InP QD shows that the primary phosphide signal resonates at ca. 15 ppm more negative shift (Figure S5). There is also an additional ^{31}P NMR signal centered at −250 ppm in the spectrum of Cd−InP (Figure 1). The ^{31}P spin-diffusion experiments on Cd−InP QD show that the more negative ^{31}P isotropic chemical shifts between −200 and −275 ppm are only observed at short spin diffusion times, confirming that the signals in this region are associated with surface and sub-surface phosphides (Figure S4). TEM images of InP and Cd−InP QD revealed that both samples have similar average particle diameters of 3.1 nm ± 0.3 nm and 2.7 nm ± 0.3 nm, respectively, consistent with prior studies, which observed similar particle diameters before and after Cd treatment.[10] Therefore, the more negative shift of the ^{31}P NMR signals in Cd−InP QD cannot be explained by changes in the diameter of the particles; rather, they must be due to alloying of some Cd into the surface or sub-surface regions of InP QD. However, as discussed below, it is not possible to directly detect ^{113}Cd NMR signals associated with phosphide-coordinated Cd atoms in Cd−InP QD.

The spatial proximity of different ^{31}P species in the MSC and QD was determined with the use of a dipolar ^{31}P double quantum single quantum (DQ-SQ) homonuclear correlation NMR experiments. The ^{31}P DQ-SQ NMR spectra were recorded using the POST-C7 recoupling scheme[36] (Figures 2 and S6). In the dipolar ^{31}P DQ-SQ correlation spectra, only ^{31}P NMR signals from spins that are dipolar coupled to other ^{31}P spins (within ca. 3−4 Å of one another) will be observed. All samples give rise to DQ-filtered ^{31}P NMR signals because all of the phosphorus atoms in the QD or MSC will be proximate to other ^{31}P spins.

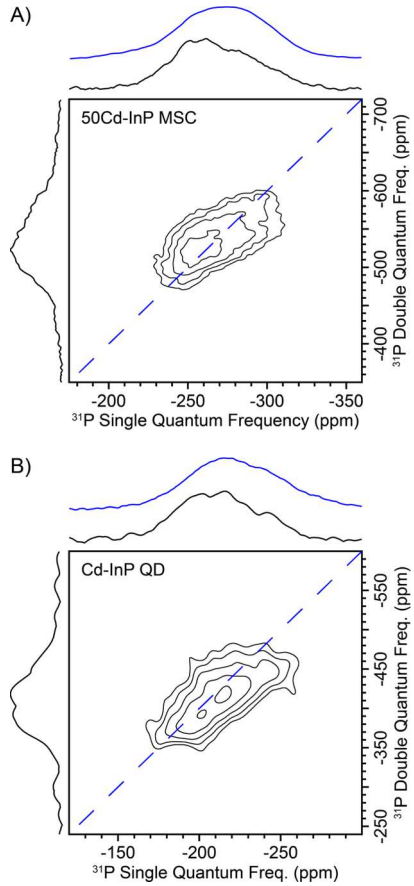

Figure 2. DNP-enhanced ^{31}P DQ-SQ 2D correlations of (A) 50Cd−InP MSC and (B) Cd−InP QD. The diagonal line indicates auto-correlations ($\delta_{SQ} = 2 \times \delta_{DQ}$). The ^{31}P CPMAS spectrum (blue trace) is overlaid on the projection of the SQ dimension. Total experiment times were 5.7 and 8 h for 50Cd−InP MSC and Cd−InP QD, respectively.

The 2D ^{31}P DQ-SQ NMR spectra show an interesting pattern. For all the samples, the 2D NMR signals primarily lie on or near the diagonal line formed when the SQ chemical shift is twice that of the DQ chemical shift. The NMR signals along this line are all auto-correlations that arise when the isotropic chemical shifts of the coupled ^{31}P spins are the same. This auto-correlation pattern is expected if ^{31}P spins within each region (e.g., core, sub-surface, and surface regions) have distinct isotropic chemical shifts. However, note that ^{31}P spins

https://dx.doi.org/10.1021/acs.jpcc.0c09601
J. Phys. Chem. C 2021, 125, 2956−2965

with the most negative chemical shifts give rise to significant 2D NMR signal intensities lying off the auto-correlation line. This observation is consistent with assignment of ^{31}P with the most negative chemical shifts to surface phosphides. The surface phosphides will be weakly coupled to other surface phosphides because they terminate the particle but should be coupled to sub-surface phosphides with a more positive isotropic chemical shift, resulting in off-diagonal signals in the 2D NMR spectra. By the same logic, core ^{31}P signals should also give rise to signals away from the auto-correlation line resulting from the coupling between core and sub-surface ^{31}P spins. Indeed, core and sub-surface correlations are visible in some of the DQ-SQ spectra (Figure S6).

The location of Cd^{2+} ions incorporated into the QD and MSC was directly probed with DNP-enhanced ^{1}H → ^{113}Cd cross-polarization Carr Purcell Meiboom Gill (CP-CPMG) NMR experiments (Figure 3). We also obtained a DNP-enhanced ^{113}Cd CP-CPMG spectrum of powdered $Cd(OA)_2$ impregnated with TEKPol TCE. $Cd(OA)_2$ was the reagent used for the Cd treatment of InP MSC and InP QD. The ^{113}Cd solid-state NMR spectrum of impregnated $Cd(OA)_2$ shows isotropic ^{113}Cd chemical shifts of −637, −671, −721, and −726 ppm, all of which are within the known range of Cd species coordinated by four to six oxygen atoms (Figures 3 and S7).[37−40] The appearance of multiple peaks likely occurs because of the complex structures associated with such metal carboxylate species and some of the $Cd(OA)_2$ may partially dissolve in the TCE TEKPol solution used for impregnation. The ^{113}Cd CP-CPMG NMR spectra of 50Cd−InP MSC and Cd−InP QD display a broad ^{113}Cd NMR signal centered at ca. −640 ppm. For 5Cd−InP MSC, no ^{113}Cd CP-CPMG NMR signal was observed, which is likely due to the lower Cd concentration in the sample. A ^{113}Cd chemical shift of −640 ppm indicates that the Cd atoms are coordinated by oxygen atoms.[37−40] Therefore, the isotropic ^{113}Cd chemical shift suggests two probable locations for the Cd^{2+} ions: (i) they are bound to both surface phosphate groups and OA ligands or (ii) there are "free" $Cd(OA)_2$ species dissolved in the polarizing agent solution or adsorbed onto the surface of MSC/QD. ^{113}Cd{^{31}P} REDOR experiments on both 50Cd−InP MSC and Cd−InP QD show slight dephasing, confirming that some of the Cd^{2+} ions are within 5−7 Å of ^{31}P spins. Furthermore, a 2D ^{31}P{^{113}Cd} D-HMQC spectrum of Cd−InP QD verifies that some of the ^{113}Cd NMR signals arise from Cd ions bound to surface phosphate groups (see below). Therefore, the REDOR experiments and ^{113}Cd chemical shifts observed in the ^{1}H → ^{113}Cd CP-CPMG spectra suggest that the majority of Cd atoms within 50Cd−InP MSC and Cd−InP QD arise from Cd atoms that are coordinated by OA ligands, with some of the Cd atoms additionally coordinated to phosphate groups on the surfaces of MSC and QD.

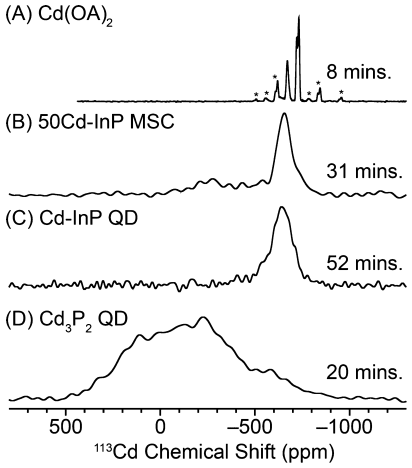

Figure 3. DNP-enhanced ^{113}Cd CP-CPMG spectra of (A) $Cd(OA)_2$ impregnated with TEKPol TCE, (B) 50Cd−InP MSC, (C) Cd−InP QD, and (D) Cd_3P_2 QD. The asterisks in (A) denote spinning sidebands. The CPMG individual echoes were co-added to obtain an absorption mode spectrum using software Nuts. Total experiment times are indicated next to each spectrum.

The ^{1}H → ^{113}Cd CP-CPMG spectrum of 50Cd−InP MSC also shows an additional, weak, and broad ^{113}Cd NMR signal centered at −280 ppm. This ^{113}Cd chemical shift is similar to that observed for Cd atoms located at the sub-surface/surface of Cd_3P_2 QD that are capped with oleate ligands (Figure 3). This signal is assigned to Cd atoms substituted into the In positions within the MSC and which are coordinated by both phosphide and OA ligands. The low intensity of ^{113}Cd NMR signals associated with Cd atoms substituted into the In positions within the MSC, as compared to the intense signals for oxygen-coordinated Cd, suggests that there may be an excess of OA-coordinated Cd atoms in 50Cd−InP MSC that are not substituted into the In positions within the MSC. However, it is also possible that Cd atoms within the MSC may be further away from the ^{1}H spins of the ligands, resulting in less effective ^{1}H → ^{113}Cd CP transfers. This is an important point to keep in mind when considering the ^{1}H → ^{113}Cd CP-CPMG NMR spectrum of Cd−InP QD. Recall that the ^{31}P chemical shifts of the surface phosphides of Cd−InP QD showed a more negative chemical shift than those of InP QD, suggesting some alloying of Cd into the sub-surface phosphide region of particles. However, these sub-surface Cd sites may be too dilute or too far from surface ^{1}H spins such that their ^{1}H → ^{113}Cd CP-CPMG NMR signals cannot be directly detected.

To probe the distance between the Cd and P atoms, ^{113}Cd{^{31}P} REDOR experiments were performed (Figure 4). ^{31}P{^{113}Cd} REDOR was also attempted and would be preferred as this experiment could directly show whether or not Cd ions are proximate to surface phosphate groups and/or if they are alloyed into the sub-surface and core regions. However, the ^{113}Cd REDOR recoupling pulses result in partial saturation of 100% abundant quadrupolar $^{113/115}$In spins. All In atoms have spin-active nuclei [NA(^{113}In) = 4.3% and NA(^{115}In) = 95.7%] and the ^{115}In and ^{113}Cd Larmor frequencies only differ by 120 kHz. ^{31}P{^{113}Cd} REDOR experiments on InP QD that were not treated with Cd showed significant dephasing, confirming that partial saturation of quadrupolar $^{113/115}$In spins is the primary source of dephasing (Figure S8). We also note that ^{31}P{^{113}Cd} REDOR is hindered by short ^{31}P refocused transverse relaxation constant (T_2') that are on the order of ca. 1 ms. For all these reasons, only ^{113}Cd{^{31}P} REDOR provided useful information. The ^{113}Cd-{^{31}P} REDOR dipolar dephasing curves were fit to analytical Bessel functions that describe the dipolar oscillation between two coupled spins.[41]

For 50Cd−InP MSC and Cd−InP QD, ^{31}P−^{113}Cd distances of approximately 5.7 and 7.0 Å, respectively, were measured by ^{113}Cd{^{31}P} REDOR. The distance measured between ^{31}P−^{113}Cd suggests that there are at least two bonds between the Cd and P atoms, that is, a P−O−Cd bonding arrangement

https://dx.doi.org/10.1021/acs.jpcc.0c09601
J. Phys. Chem. C 2021, 125, 2956−2965

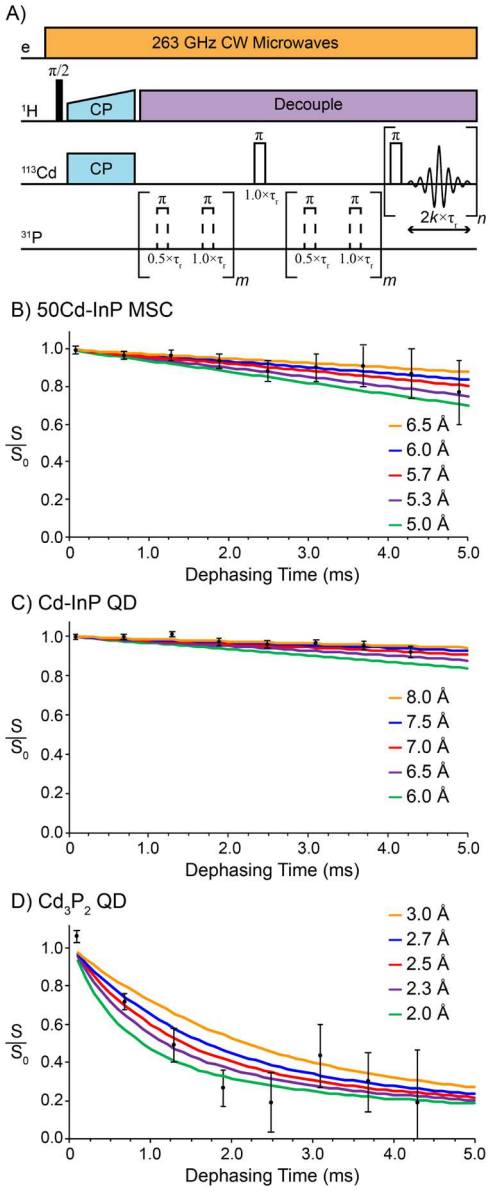

Figure 4. (A) DNP-enhanced $^{113}Cd\{^{31}P\}$ REDOR with CPMG detection pulse sequence. (B–D) Experimentally obtained $^{113}Cd\{^{31}P\}$ REDOR curves of (B) 50Cd–InP MSC, (C) Cd–InP QD, and (D) Cd_3P_2 QD with simulated fits. Simulated REDOR curves are shown for the indicated ^{113}Cd–^{31}P inter-nuclear distances. ^{113}Cd–^{31}P inter-nuclear distances of 2.0 and 8.0 Å correspond to dipolar coupling constants of −1356 and −21 Hz, respectively. Each REDOR curve required between 4.6 and 12.6 h to acquire (see Table S2).

due to binding of Cd to surface phosphate groups (Scheme 1). The large measured distances could also reflect the fact that some of the Cd^{2+} ions are far from surface phosphates or phosphides, resulting in apparent lengthening of the ^{113}Cd–^{31} P internuclear distances. Binding of Cd to some surface phosphate groups is consistent with the observation made from the ^{31}P CPMAS NMR spectra that during the post-synthetic treatment of InP QD and MSC, surface phosphates are being formed. If the $Cd^{113}Cd$ NMR signals arose from Cd alloyed into the core of the InP QD or MSC, the observed dephasing would be more much more rapid, as is observed in the $^{113}Cd\{^{31}P\}$ REDOR experiment of Cd_3P_2 QD (Figure 4). For Cd_3P_2 QD, a ^{113}Cd–^{31}P inter-nuclear distance of 2.5 Å was estimated from fits of the initial portion of the $^{113}Cd\{^{31}P\}$ REDOR curve. This distance is consistent with the Cd–P bond distance of 2.6 Å measured using single-crystal X-ray diffraction.[42]

In addition to the $^{113}Cd\{^{31}P\}$ REDOR experiments, a $^{31}P\{^{113}Cd\}$ constant time D-HMQC experiment was performed on the Cd–InP QD (Figure 5A). For the $^{31}P\{^{113}Cd\}$ D-HMQC experiment, a second batch of Cd–InP QD was used and had a DNP enhancement of ca. 53. The ^{113}Cd and ^{31}P solid-state NMR spectra of the second batch of Cd–InP QD are nearly identical to the spectra from the first batch, except that the phosphate ^{31}P NMR signal has a slightly larger relative intensity, as compared to the phosphide signals (Figure S9). The 2D $^{31}P\{^{113}Cd\}$ D-HMQC spectrum of Cd–InP QD shows correlations between the phosphate groups and a broad ^{113}Cd NMR signal centered at ca. −700 ppm and a second, narrower ^{113}Cd NMR signal at −800 ppm. Phosphide ^{31}P NMR signals are likely absent from the 2D D-HMQC spectrum because of their shorter T_2'. A comparison of the ^{113}Cd NMR spectrum obtained from the D-HMQC spectrum and the directly detected ^{113}Cd CP-CPMG NMR spectrum shows that there are some visible differences in ^{113}Cd chemical shifts and peak intensities. The ^{113}Cd NMR signal at −800 ppm has a very low intensity in the ^{113}Cd CP-CPMG spectrum, suggesting that it corresponds to Cd ions that are distant from ^{1}H spins and/or dilute but must be associated with phosphate groups; these Cd ions could be coordinated by phosphate and/or surface oxide anions. The high-frequency ^{113}Cd NMR signals centered at −650 ppm observed in the CP-CPMG spectrum have greatly reduced intensity in the D-HMQC spectrum. Therefore, these signals are assigned to Cd ions that are coordinated by oleate ligands but are distant from phosphate groups. It is known that cadmium dicarboxylate fragments often act as Z-type ligands, which can reversibly associate with the surface of nanoparticles.[43−45] The remaining ^{113}Cd NMR signals centered at −700 ppm could then arise from Cd ions that are coordinated to both oleate ligands and surface phosphate groups.

CONCLUSIONS

Through examination of a series of InP MSC with various amounts of Cd incorporated, InP QD, and Cd_3P_2 QD, it was possible to determine the location of Cd atoms in post-synthetic Cd–InP QD using DNP-enhanced ^{31}P and ^{113}Cd solid-state NMR experiments. Scheme 1 summarizes the findings of this study. DNP-enhanced ^{113}Cd CP-CPMG NMR spectra, $^{113}Cd\{^{31}P\}$ REDOR spectra, and $^{31}P\{^{113}Cd\}$ D-HMQC confirm that most Cd atoms are coordinated to oxygen-bearing ligands, either oleate ligands and/or phosphate groups. The $^{31}P\{^{113}Cd\}$ D-HMQC and $^{113}Cd\{^{31}P\}$ REDOR experiments suggest that only a subset of Cd ions are bound to surface phosphate groups. However, while ^{113}Cd NMR experiments could not provide direct evidence for alloying of Cd into the phosphide regions, a comparison of ^{31}P chemical shifts of the QD and MSC samples indirectly suggested that some alloying of Cd has occurred. The structural model put forward on the basis of solid-state NMR experiments is consistent with previous characterization of Cd–InP QDs by cadmium EXAFS, which demonstrated Cd–O and Cd–P coordination.[10] More generally, this study highlights the utility of DNP SENS for the characterization of QD and other nanomaterials.[19−29,46−52]

https://dx.doi.org/10.1021/acs.jpcc.0c09601
J. Phys. Chem. C 2021, 125, 2956−2965

Scheme 1. Proposed Model of the Surface of Cd−InP QD Depicting the Possible Location of Cd Ions and Different Surface Species

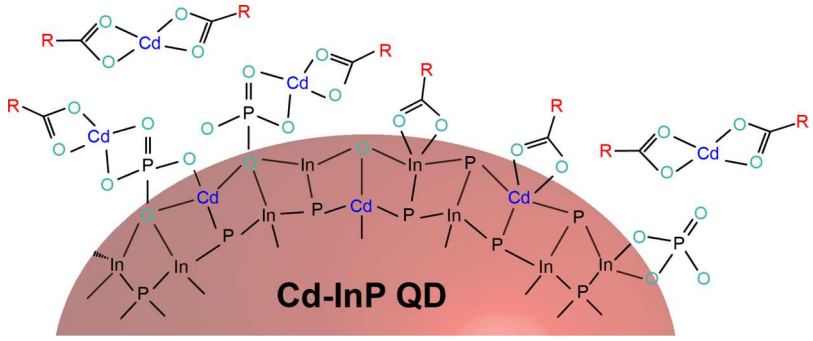

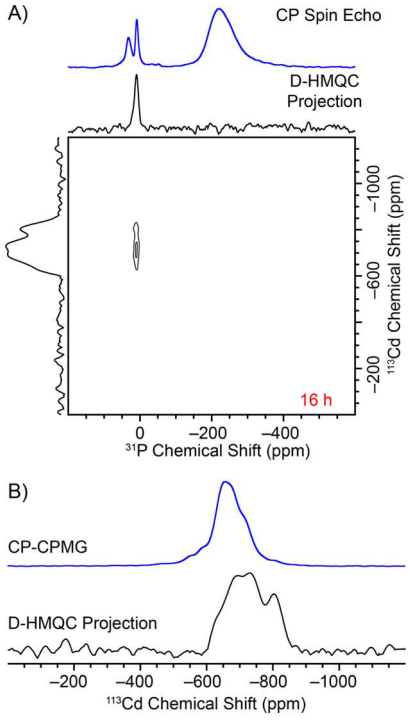

Figure 5. (A) DNP-enhanced $^{31}P\{^{113}Cd\}$ constant time D-HMQC of Cd−InP QD. The spectrum was acquired with a MAS frequency of 10 kHz with REDOR recoupling applied on the ^{113}Cd channel. The top spectrum is the 1D ^{31}P CP spin echo of Cd−InP QD. (B) Comparison of ^{113}Cd CP-CPMG spectrum and ^{113}Cd projection extracted from the indirect dimension of the $^{31}P\{^{113}Cd\}$ D-HMQC spectrum.

EXPERIMENTAL SECTION

General Considerations. All glassware was dried in a 160 °C oven overnight prior to use. All reactions, unless otherwise noted, were performed under an inert atmosphere of nitrogen using a glovebox or standard Schlenk techniques. Indium acetate (99.99%), anhydrous oleic acid (≥99%), and anhydrous acetonitrile were purchased from MilliporeSigma and used without further purification. Toluene purchased from MilliporeSigma was collected from a solvent purification system and stored over activated 3 Å molecular sieves in a glovebox. 1-Octadecene (1-ODE, 90%) was purchased from MilliporeSigma, dried over CaH_2, distilled, and stored over activated 3 Å molecular sieves in a nitrogen atmosphere glovebox. Dimethyl cadmium (97%) was purchased from Strem Chemicals and stored in a −35 °C freezer in a nitrogen-filled glovebox. Tris(trimethylsilyl)phosphine $[P(SiMe_3)_3]$ was prepared by modifying a literature procedure in which sodium naphthalene was used in place of Na/K alloy.[53] Cadmium oleate was prepared following a literature procedure.[10] Bio-Beads S-X1 for gel permeation chromatography were purchased from Bio-Rad Laboratories and dried under vacuum at elevated temperatures before being stored in a glovebox. OmniTrace nitric acid was purchased from MilliporeSigma and used without further purification. 18 MΩ water was collected from the MilliporeSigma water purification system. ICP-OES was performed using a PerkinElmer Optima 8300.

Synthesis of InP MSC. Oleate-capped InP MSC were synthesized using an adapted procedure published by Gary et al.[54] Briefly, indium acetate (937 mg, 3.2 mmol) and oleic acid (3.28 g, 11.6 mmol) were stirred overnight at 110 °C under reduced pressure. Anhydrous toluene (20 mL) was added to the reaction flask at room temperature to dissolve indium oleate, followed by $P(SiMe_3)_3$ (465 μL, 1.6 mmol) suspended in 10 mL anhydrous toluene, at 110 °C. Cluster growth is typically complete within 20−40 min. Purification was done in a N_2-filled glovebox by repeated precipitation/redissolution cycles using toluene and acetonitrile as the solvent and anti-solvent, respectively. The purified material was stored as a solid in a N_2-filled glovebox.

Cadmium Treatment of InP MSC. Following a published procedure,[14] Cd−InP MSC samples were prepared by first dissolving 0.187 g (0.0097 mmol) of oleate-capped InP MSC in 2 mL of toluene in a 20 mL scintillation vial containing a stir bar. To this solution was added 0.329 g (0.487 mmol, 50 equivalents of Cd relative to In in the cluster) of cadmium oleate dissolved in 5 mL of toluene. The solution was stirred for 20 h at room temperature and then concentrated to 4 mL. Acetonitrile (5 mL) was added and the suspension was centrifuged (7000 rpm for 10 min). The solid precipitate was redissolved in toluene and purified twice using gel permeation chromatography in the glovebox following literature procedures.[55,56] The procedure outlined above was repeated a second time with 5 equivalents of Cd per equivalent of In. The duration of the reaction was between 20 and 72 h.

Synthesis of InP QD. InP QD were synthesized following published methods.[10,57] Briefly, a stock solution of InP QD was synthesized starting from indium acetate (1.17 g, 4 mmol) and oleic acid (4.10 g, 14.5 mmol) in 1-octadecene (4 g) degassed at 100 °C overnight. Upon heating the reaction flask to 315 °C in N_2 flow, $P(SiMe_3)_3$ (2 mmol) suspended in 1-octadecene (4 g) was injected. Alternatively, oleate-capped InP MSC (234 mg, 12 mmol) were dissolved in anhydrous 1-octadecene (5 mL) and injected into a flask containing 35 mL of 1-

https://dx.doi.org/10.1021/acs.jpcc.0c09601
J. Phys. Chem. C 2021, 125, 2956−2965

octadecene at 300 °C. The reaction is typically complete in 15−20 min. To start purification, 1-octadecene was removed through vacuum distillation at elevated temperatures (∼160 °C) and taken into a N_2-filled glovebox, followed by repeated precipitation/redissolution cycles using toluene and acetonitrile as the solvent and anti-solvent, respectively. For further purification, gel permeation chromatography was performed in a glovebox following literature procedures.[55,56] Purified material was stored as a stock solution in toluene in a N_2-filled glovebox. QD solids were isolated by removing the solvent under reduced pressure with a glovebox-attached cold trap.

Cadmium Treatment of InP QD. The Cd−InP QD sample was prepared using a published procedure.[10] Cadmium oleate (270 mg, 0.4 mmol, 2 equivalents to mmol In^{3+} estimated to be present in the QD stock) was dissolved in anhydrous dodecane (5 mL) and injected into the reaction flask containing InP QD suspended in 5 mL of dodecane. The use of dodecane here was for ease of purification by vacuum distillation. The solution was heated to 200 °C, and the reaction was halted by removing the heating mantle at 90 min when no further changes in the absorbance or PL features were observed. The resulting QD were purified following the same purification steps as InP QD.

Synthesis of Cd_3P_2 QD. Dimethyl cadmium being a volatile and extremely toxic reactant was handled with care within a N_2-filled glovebox. Both dimethyl cadmium and $P(SiMe_3)_3$ are pyrophoric, extremely reactive, and should be handled with caution. Cd_3P_2 QD were synthesized following published methods.[27,58] Briefly, cadmium oleate (0.55 g, 0.8 mmol), oleic acid (0.5 mL, 1.58 mmol), and 1-octadecene (10 mL) were combined and heated to 150 °C with stirring. $P(SiMe_3)_3$ (60 μL, 0.2 mmol) in 1 mL of 1-octadecene was rapidly injected into the flask. After 3 min, the solution was cooled by placing the flask in an oil bath. The resulting QD were purified following the same purification steps as InP QD.

Structural Characterization of QDs and Measurement of Particle Diameters. InP, Cd−InP, and Cd_3P_2 QD were characterized by UV−Vis absorption and emission spectroscopy, TEM imaging, and powder X-ray diffraction (Figures S10−S12). Average particle diameters determined by analysis of TEM images were 3.1 nm ± 0.3 nm, 2.7 nm ± 0.3 nm, and 2.2 nm ± 0.3 nm for InP, Cd−InP, and Cd_3P_2 QD, respectively.

Solid-State NMR Experiments. TCE (Sigma-Aldrich),[59] *h*-BN (Sigma-Aldrich), and TEKPol[60] (CortecNet) were purchased from commercial suppliers. Samples were prepared for DNP experiments in two different ways. In both cases, *h*-BN was used as a material to disperse the QD or MSC and keep them mixed with the radical polarizing agent.[24,27] Samples were prepared by impregnating 30 mg of *h*-BN with approximately 20 μL of colloidal QD/MSC solution and 10 μL of 40 mM TEKPol TCE solution, then transferring the impregnated *h*-BN to a sapphire rotor. This composition gives a final TEKPol concentration of approximately 16 mM. Other samples were prepared by evaporating the colloidal solution to obtain precipitated QD. A 1:1 mass of the precipitated QD and *h*-BN powders were mixed, then the powdered mixture was impregnated with a small volume (10−20 μL) of 16 mM TEKPol solution.[27] Figure captions indicate which sample preparation method was used for each spectrum. Unless noted, all InP MSC, QD, and Cd_3P_2 samples were handled in a glovebox to prevent oxidation, and impregnation was performed with dried TCE.

All DNP solid-state NMR experiments were performed on a Bruker 9.4 T 400 MHz/263 GHz solid-state NMR/gyrotron equipped with an AVANCE III console.[17] The main magnetic field was set on a standard sample of TEKPol TCE solution so that microwave irradiation gave a maximum positive DNP enhancement. A Bruker 3.2 mm triple resonance HXY probe was used and configured to $^{1}H-^{31}P-^{113}Cd$ mode. Samples were packed into 3.2 mm sapphire rotors and capped with Teflon inserts (for samples prepared in air) or silica plugs (for samples prepared under inert conditions). Zirconia drive caps were used in all cases. All samples were spun at 10 kHz and the sample temperature was approximately 110 K under microwave irradiation. All DNP-enhanced NMR spectra were indirectly referenced using previously published relative NMR frequencies.[61] The CP-spin echo, CP-total suppression of spinning sidebands,[62] homonuclear dipolar DQ-SQ with post-C7 recoupling,[36] CP-CPMG,[63] REDOR,[64] and constant time[65] CP-D-HMQC[27,66] experiments were performed using previously published pulse sequences. While performing the experiments ^{1}H high-power decoupling was performed with the SPINAL-64 scheme[67] and the ^{1}H radiofrequency (rf) field was 100 kHz. All key solid-state NMR experimental parameters are presented in Table S2.

^{31}P pulses were directly calibrated on an air-exposed Cd−InP QD sample. The ^{31}P CP match condition used ^{1}H and ^{31}P spinlock rf fields of 40 kHz and 50 kHz, respectively. The CP spinlock duration was between 2 and 9 ms and was experimentally optimized on each sample to maximize the phosphide signal. The conditions used for each experiment are listed in Table S2. The ^{31}P π pulse used for the CPMAS spin echo experiments was 7 μs (72 kHz rf field). ^{113}Cd pulses were calibrated on the $Cd(OA)_2$ precursor that was used to treat the surface of the InP QD and MSC samples. The ^{113}Cd CP match condition used ^{1}H and ^{113}Cd spinlock rf fields of 63−77 and 64−71 kHz, respectively, and the CP spinlock duration was optimized on each sample and is noted in Table S2. The ^{113}Cd π pulse rf field was 64−77 kHz for all experiments. The REDOR recoupling pulses were phase-cycled with XY-8 scheme to compensate for pulse imperfections and offsets. In the $^{113}Cd\{^{31}P\}$ REDOR experiments, the ^{31}P REDOR recoupling π pulse rf field was 72 kHz, and in the $^{31}P\{^{113}Cd\}$ REDOR experiments, the ^{113}Cd REDOR recoupling π pulse rf field was 60 kHz. Finally, for the $^{31}P\{^{113}Cd\}$ constant time D-HMQC, the indirect dimension was set wide enough to obtain the entire ^{113}Cd spectrum (250 kHz), and the REDOR recoupling was applied on the ^{113}Cd channel where the ^{113}Cd rf field was 77 kHz.

■ ASSOCIATED CONTENT

Supporting Information

The Supporting Information is available free of charge at https://pubs.acs.org/doi/10.1021/acs.jpcc.0c09601.

Experimental procedures; ^{31}P peak fit parameters; NMR experimental parameters; DNP-enhanced ^{31}P CPMAS spectra of Cd−InP QD prepared under air-free and ambient conditions; DNP-enhanced ^{31}P CPMAS spin diffusion spectra of InP QD, 50Cd−InP MSC, and Cd−InP QD; comparison DNP-enhanced ^{31}P CPMAS spectra of InP QD, Cd−InP QD, and Cd_3P_2 QD; ^{31}P D-HMQC spectra of InP QD, Cd_3P_2 QD, InP MSC, and

https://dx.doi.org/10.1021/acs.jpcc.0c09601
J. Phys. Chem. C 2021, 125, 2956−2965

5Cd−InP MSC; ^{113}Cd solid-state NMR spectra of $Cd(OA)_2$; $^{31}P\{^{113}Cd\}$ REDOR control experiments on InP QD; comparison of DNP-enhanced ^{31}P CP-spin echo spectra of two different batches of Cd−InP QD; UV-Vis absorption and emission spectra, TEM images, and PXRD patterns of InP QD, Cd−InP QD, and Cd_3P_2 QD (PDF)

AUTHOR INFORMATION

Corresponding Authors

Brandi M. Cossairt − *Department of Chemistry, University of Washington, Seattle, Washington 98195, United States;* orcid.org/0000-0002-9891-3259; Phone: 206-543-4643; Email: cossairt@chem.washington.edu

Aaron J. Rossini − *Department of Chemistry, Iowa State University, Ames, Iowa 50011, United States; U.S. DOE Ames Laboratory, Ames, Iowa 50011, United States;* orcid.org/0000-0002-1679-9203; Phone: 515-294-8952; Email: arossini@iastate.edu

Authors

Michael P. Hanrahan − *Department of Chemistry, Iowa State University, Ames, Iowa 50011, United States; U.S. DOE Ames Laboratory, Ames, Iowa 50011, United States*

Jennifer L. Stein − *Department of Chemistry, University of Washington, Seattle, Washington 98195, United States;* orcid.org/0000-0002-6553-5116

Nayon Park − *Department of Chemistry, University of Washington, Seattle, Washington 98195, United States*

Complete contact information is available at: https://pubs.acs.org/10.1021/acs.jpcc.0c09601

Notes

The authors declare no competing financial interest.

ACKNOWLEDGMENTS

DNP-NMR experiments (MPH and AJR) were supported by the U.S. Department of Energy (DOE), Office of Science, Basic Energy Sciences, Materials Science and Engineering Division. The Ames Laboratory operated for the U.S. DOE by Iowa State University under contract # DE-AC02-07CH11358. AJR acknowledges additional support from the Alfred P. Sloan Foundation through a Sloan research fellowship. Synthesis of InP QD and MSC samples was supported by the National Science Foundation through the CAREER program (BC and JLS, CHE-1552164), and cadmium doping studies were supported by the UW Molecular Engineering Materials Center, a Materials Research Science and Engineering Center (JLS and NP, DMR-1719797).

REFERENCES

(1) Kovalenko, M. V.; Manna, L.; Cabot, A.; Hens, Z.; Talapin, D. V.; Kagan, C. R.; Klimov, V. I.; Rogach, A. L.; Reiss, P.; Milliron, D. J.; et al. Prospects of Nanoscience with Nanocrystals. *ACS Nano* **2015**, *9*, 1012−1057.

(2) Reiss, P.; Carrière, M.; Lincheneau, C.; Vaure, L.; Tamang, S. Synthesis of Semiconductor Nanocrystals, Focusing on Nontoxic and Earth-Abundant Materials. *Chem. Rev.* **2016**, *116*, 10731−10819.

(3) Harris, D. K.; Bawendi, M. G. Improved Precursor Chemistry for the Synthesis of III-V Quantum Dots. *J. Am. Chem. Soc.* **2012**, *134*, 20211−20213.

(4) Cui, J.; Beyler, A. P.; Marshall, L. F.; Chen, O.; Harris, D. K.; Wanger, D. D.; Brokmann, X.; Bawendi, M. G. Direct Probe of Spectral Inhomogeneity Reveals Synthetic Tunability of Single-Nanocrystal Spectral Linewidths. *Nat. Chem.* **2013**, *5*, 602−606.

(5) Tamang, S.; Lincheneau, C.; Hermans, Y.; Jeong, S.; Reiss, P. Chemistry of InP Nanocrystal Syntheses. *Chem. Mater.* **2016**, *28*, 2491−2506.

(6) Brown, R. P.; Gallagher, M. J.; Fairbrother, D. H.; Rosenzweig, Z. Synthesis and Degradation of Cadmium-Free InP and InPZn/ZnS Quantum Dots in Solution. *Langmuir* **2018**, *34*, 13924−13934.

(7) Xu, Z.; Li, Y.; Li, J.; Pu, C.; Zhou, J.; Lv, L.; Peng, X. Formation of Size-Tunable and Nearly Monodisperse InP Nanocrystals: Chemical Reactions and Controlled Synthesis. *Chem. Mater.* **2019**, *31*, 5331−5341.

(8) Xie, R.; Battaglia, D.; Peng, X. Colloidal InP Nanocrystals as Efficient Emitters Covering Blue to near-Infrared. *J. Am. Chem. Soc.* **2007**, *129*, 15432−15433.

(9) Xu, S.; Ziegler, J.; Nann, T. Rapid Synthesis of Highly Luminescent InP and InP/ZnS Nanocrystals. *J. Mater. Chem.* **2008**, *18*, 2653−2656.

(10) Stein, J. L.; Mader, E. A.; Cossairt, B. M. Luminescent Inp Quantum Dots with Tunable Emission by Post-Synthetic Modification with Lewis Acids. *J. Phys. Chem. Lett.* **2016**, *7*, 1315−1320.

(11) Tomaselli, M.; Yarger, J. L.; Bruchez, M.; Havlin, R. H.; deGraw, D.; Pines, A.; Alivisatos, A. P. NMR Study of InP Quantum Dots: Surface Structure and Size Effects. *J. Chem. Phys.* **1999**, *110*, 8861−8864.

(12) Cros-Gagneux, A.; Delpech, F.; Nayral, C.; Cornejo, A.; Coppel, Y.; Chaudret, B. Surface Chemistry of InP Quantum Dots: A Comprehensive Study. *J. Am. Chem. Soc.* **2010**, *132*, 18147−18157.

(13) Virieux, H.; Le Troedec, M.; Cros-Gagneux, A.; Ojo, W.-S.; Delpech, F.; Nayral, C.; Martinez, H.; Chaudret, B. InP/ZnS Nanocrystals: Coupling NMR and XPS for Fine Surface and Interface Description. *J. Am. Chem. Soc.* **2012**, *134*, 19701−19708.

(14) Stein, J. L.; Steimle, M. I.; Terban, M. W.; Petrone, A.; Billinge, S. J. L.; Li, X.; Cossairt, B. M. Cation Exchange Induced Transformation of InP Magic-Sized Clusters. *Chem. Mater.* **2017**, *29*, 7984−7992.

(15) Tessier, M. D.; Baquero, E. A.; Dupont, D.; Grigel, V.; Bladt, E.; Bals, S.; Coppel, Y.; Hens, Z.; Nayral, C.; Delpech, F. Interfacial Oxidation and Photoluminescence of InP-Based Core/Shell Quantum Dots. *Chem. Mater.* **2018**, *30*, 6877−6883.

(16) Stein, J. L.; Holden, W. M.; Venkatesh, A.; Mundy, M. E.; Rossini, A. J.; Seidler, G. T.; Cossairt, B. M. Probing Surface Defects of InP Quantum Dots Using Phosphorus Kα and Kß X-Ray Emission Spectroscopy. *Chem. Mater.* **2018**, *30*, 6377−6388.

(17) Rosay, M.; Tometich, L.; Pawsey, S.; Bader, R.; Schauwecker, R.; Blank, M.; Borchard, P. M.; Cauffman, S. R.; Felch, K. L.; Weber, R. T.; et al. Solid-State Dynamic Nuclear Polarization at 263 GHz: Spectrometer Design and Experimental Results. *Phys. Chem. Chem. Phys.* **2010**, *12*, 5850−5860.

(18) Ni, Q. Z.; Daviso, E.; Can, T. V.; Markhasin, E.; Jawla, S. K.; Swager, T. M.; Temkin, R. J.; Herzfeld, J.; Griffin, R. G. High Frequency Dynamic Nuclear Polarization. *Acc. Chem. Res.* **2013**, *46*, 1933−1941.

(19) Lesage, A.; Lelli, M.; Gajan, D.; Caporini, M. A.; Vitzthum, V.; Miéville, P.; Alauzun, J.; Roussey, A.; Thieuleux, C.; Mehdi, A.; et al. Surface Enhanced NMR Spectroscopy by Dynamic Nuclear Polarization. *J. Am. Chem. Soc.* **2010**, *132*, 15459−15461.

(20) Lafon, O.; Thankamony, A. S. L.; Rosay, M.; Aussenac, F.; Lu, X.; Trébosc, J.; Bout-Roumazeilles, V.; Vezin, H.; Amoureux, J.-P. Indirect and Direct ^{29}Si Dynamic Nuclear Polarization of Dispersed Nanoparticles. *Chem. Commun.* **2013**, *49*, 2864−2866.

(21) Akbey, Ü.; Altin, B.; Linden, A.; Özçelik, S.; Gradzielski, M.; Oschkinat, H. Dynamic Nuclear Polarization of Spherical Nanoparticles. *Phys. Chem. Chem. Phys.* **2013**, *15*, 20706−20716.

(22) Protesescu, L.; Rossini, A. J.; Kriegner, D.; Valla, M.; de Kergommeaux, A.; Walter, M.; Kravchyk, K. V.; Nachtegaal, M.; Stangl, J.; Malaman, B.; et al. Unraveling the Core-Shell Structure of Ligand-Capped Sn/SnO_x Nanoparticles by Surface-Enhanced Nuclear

Magnetic Resonance, Mossbauer, and X-Ray Absorption Spectroscopies. *ACS Nano* **2014**, *8*, 2639−2648.
(23) Kobayashi, T.; Perras, F. A.; Slowing, I. I.; Sadow, A. D.; Pruski, M. Dynamic Nuclear Polarization Solid-State NMR in Heterogeneous Catalysis Research. *ACS Catal.* **2015**, *5*, 7055−7062.
(24) Piveteau, L.; Ong, T.-C.; Rossini, A. J.; Emsley, L.; Copéret, C.; Kovalenko, M. V. Structure of Colloidal Quantum Dots from Dynamic Nuclear Polarization Surface Enhanced NMR Spectroscopy. *J. Am. Chem. Soc.* **2015**, *137*, 13964−13971.
(25) Viger-Gravel, J.; Berruyer, P.; Gajan, D.; Basset, J.-M.; Lesage, A.; Tordo, P.; Ouari, O.; Emsley, L. Frozen Acrylamide Gels as Dynamic Nuclear Polarization Matrices. *Angew. Chem., Int. Ed.* **2017**, *56*, 8726−8730.
(26) Piveteau, L.; Ong, T.-C.; Walder, B. J.; Dirin, D. N.; Moscheni, D.; Schneider, B.; Bär, J.; Protesescu, L.; Masciocchi, N.; Guagliardi, A.; et al. Resolving the Core and the Surface of CdSe Quantum Dots and Nanoplatelets Using Dynamic Nuclear Polarization Enhanced PASS−PIETA NMR Spectroscopy. *ACS Cent. Sci.* **2018**, *4*, 1113−1125.
(27) Hanrahan, M. P.; Chen, Y.; Blome-Fernández, R.; Stein, J. L.; Pach, G. F.; Adamson, M. A. S.; Neale, N. R.; Cossairt, B. M.; Vela, J.; Rossini, A. J. Probing the Surface Structure of Semiconductor Nanoparticles by DNP SENS with Dielectric Support Materials. *J. Am. Chem. Soc.* **2019**, *141*, 15532−15546.
(28) Piveteau, L.; Dirin, D. N.; Gordon, C. P.; Walder, B. J.; Ong, T.-C.; Emsley, L.; Copéret, C.; Kovalenko, M. V. Colloidal-Ald-Grown Core/Shell Cdse/Cds Nanoplatelets as Seen by DNP Enhanced PASS−PIETA NMR Spectroscopy. *Nano Lett.* **2020**, *20*, 3003−3018.
(29) Dorn, R. W.; Ryan, M. J.; Kim, T.-H.; Goh, T. W.; Venkatesh, A.; Heintz, P. M.; Zhou, L.; Huang, W.; Rossini, A. J. Identifying the Molecular Edge Termination of Exfoliated Hexagonal Boron Nitride Nanosheets with Solid-State NMR Spectroscopy and Plane-Wave DFT Calculations. *Chem. Mater.* **2020**, *32*, 3109−3121.
(30) Cadars, S.; Smith, B. J.; Epping, J. D.; Acharya, S.; Belman, N.; Golan, Y.; Chmelka, B. F. Atomic Positional Versus Electronic Order in Semiconducting ZnSe Nanoparticles. *Phys. Rev. Lett.* **2009**, *103*, 136802.
(31) Björgvinsdóttir, S.; Walder, B. J.; Pinon, A. C.; Emsley, L. Bulk Nuclear Hyperpolarization of Inorganic Solids by Relay from the Surface. *J. Am. Chem. Soc.* **2018**, *140*, 7946−7951.
(32) Tomaselli, M.; deGraw, D.; Yarger, J. L.; Augustine, M. P.; Pines, A. Scalar and Anisotropic *J* Interactions in Undoped InP: A Triple-Resonance NMR Study. *Phys. Rev. B: Condens. Matter Mater. Phys.* **1998**, *58*, 8627−8633.
(33) Thayer, A. M.; Steigerwald, M. L.; Duncan, T. M.; Douglass, D. C. NMR Study of Semiconductor Molecular Clusters. *Phys. Rev. Lett.* **1988**, *60*, 2673−2676.
(34) Lovingood, D. D.; Achey, R.; Paravastu, A. K.; Strouse, G. F. Size- and Site-Dependent Reconstruction in CdSe QDs Evidenced by 77Se{1H} CP-MAS NMR Spectroscopy. *J. Am. Chem. Soc.* **2010**, *132*, 3344−3354.
(35) Yesinowski, J. P. Solid-State NMR of Inorganic Semiconductors. In *Topics in Current Chemistry*; Chan, J. C. C., Ed.; Springer Berlin Heidelberg: Berlin, Heidelberg, 2012; Vol. *306*; pp 229−312.
(36) Hohwy, M.; Jakobsen, H. J.; Edén, M.; Levitt, M. H.; Nielsen, N. C. Broadband Dipolar Recoupling in the Nuclear Magnetic Resonance of Rotating Solids: A Compensated C7 Pulse Sequence. *J. Chem. Phys.* **1998**, *108*, 2686−2694.
(37) Dusold, S.; Kümmerlen, J.; Schaller, T.; Sebald, A.; Dollase, W. A. A ^{31}P Spin Diffusion and ^{31}P-^{113}Cd CP/MAS NMR Study of Polycrystalline $Cd_3(PO_4)_2$. *J. Phys. Chem. B* **1997**, *101*, 6359−6366.
(38) Duncan, T. M. *A Compilation of Chemical Shift Anisotropies*; Farragut Press, 1990.
(39) Saxena, P.; Thirupathi, N. Reactions of $Cd(OAc)_2$ $2H_2O$ with Variously Substituted Pyridines. Efforts to Unravel the Factors That Determine Structure/Nuclearity of the Products. *Polyhedron* **2015**, *98*, 238−250.
(40) Frost, J. M.; Kobera, L.; Pialat, A.; Zhang, Y.; Southern, S. A.; Gabidullin, B.; Bryce, D. L.; Murugesu, M. From Discrete Molecule, to Polymer, to MOF: Mapping the Coordination Chemistry of Cd^{ii} Using ^{113}Cd Solid-State NMR. *Chem. Commun.* **2016**, *52*, 10680−10683.
(41) Mueller, K. T. Analytic Solutions for the Time Evolution of Dipolar-Dephasing NMR Signals. *J. Magn. Reson., Ser. A* **1995**, *113*, 81−93.
(42) Zanin, I. E.; Aleinikova, K. B.; Antipin, M. Y.; Afanasiev, M. M. The Structure of the Compound Cd_3P_2. *J. Struct. Chem.* **2006**, *47*, 78−81.
(43) Frederick, M. T.; Achtyl, J. L.; Knowles, K. E.; Weiss, E. A.; Geiger, F. M. Surface-Amplified Ligand Disorder in CdSe Quantum Dots Determined by Electron and Coherent Vibrational Spectroscopies. *J. Am. Chem. Soc.* **2011**, *133*, 7476−7481.
(44) Anderson, N. C.; Hendricks, M. P.; Choi, J. J.; Owen, J. S. Ligand Exchange and the Stoichiometry of Metal Chalcogenide Nanocrystals: Spectroscopic Observation of Facile Metal-Carboxylate Displacement and Binding. *J. Am. Chem. Soc.* **2013**, *135*, 18536−18548.
(45) Owen, J. The Coordination Chemistry of Nanocrystal Surfaces. *Science* **2015**, *347*, 615.
(46) Lafon, O.; Rosay, M.; Aussenac, F.; Lu, X.; Trébosc, J.; Cristini, O.; Kinowski, C.; Touati, N.; Vezin, H.; Amoureux, J.-P. Beyond the Silica Surface by Direct Silicon-29 Dynamic Nuclear Polarization. *Angew. Chem., Int. Ed.* **2011**, *50*, 8367−8370.
(47) Lafon, O.; Thankamony, A. S. L.; Kobayashi, T.; Carnevale, D.; Vitzthum, V.; Slowing, I. I.; Kandel, K.; Vezin, H.; Amoureux, J.-P.; Bodenhausen, G.; et al. Mesoporous Silica Nanoparticles Loaded with Surfactant: Low Temperature Magic Angle Spinning ^{13}C and ^{29}Si NMR Enhanced by Dynamic Nuclear Polarization. *J. Phys. Chem. C* **2013**, *117*, 1375−1382.
(48) Lee, D.; Duong, N. T.; Lafon, O.; De Paëpe, G. Primostrato Solid-State NMR Enhanced by Dynamic Nuclear Polarization: Pentacoordinated Al^{3+} Ions Are Only Located at the Surface of Hydrated Γ-Alumina. *J. Phys. Chem. C* **2014**, *118*, 25065−25076.
(49) Eedugurala, N.; Wang, Z.; Chaudhary, U.; Nelson, N.; Kandel, K.; Kobayashi, T.; Slowing, I. I.; Pruski, M.; Sadow, A. D. Mesoporous Silica-Supported Amidozirconium-Catalyzed Carbonyl Hydroboration. *ACS Catal.* **2015**, *5*, 7399−7414.
(50) Presti, C.; Thankamony, A. S. L.; Alauzun, J. G.; Mutin, P. H.; Carnevale, D.; Lion, C.; Vezin, H.; Laurencin, D.; Lafon, O. NMR and EPR Characterization of Functionalized Nanodiamonds. *J. Phys. Chem. C* **2015**, *119*, 12408−12422.
(51) Hope, M. A.; Halat, D. M.; Magusin, P. C. M. M.; Paul, S.; Peng, L.; Grey, C. P. Surface-Selective Direct ^{17}O DNP NMR of CeO_2 Nanoparticles. *Chem. Commun.* **2017**, *53*, 2142−2145.
(52) Ha, M.; Thiessen, A. N.; Sergeyev, I. V.; Veinot, J. G. C.; Michaelis, V. K. Endogenous Dynamic Nuclear Polarization NMR of Hydride-Terminated Silicon Nanoparticles. *Solid State Nucl. Magn.* **2019**, *100*, 77−84.
(53) Gary, D. C.; Cossairt, B. M. Role of Acid in Precursor Conversion During InP Quantum Dot Synthesis. *Chem. Mater.* **2013**, *25*, 2463−2469.
(54) Gary, D. C.; Terban, M. W.; Billinge, S. J. L.; Cossairt, B. M. Two-Step Nucleation and Growth of InP Quantum Dots Via Magic-Sized Cluster Intermediates. *Chem. Mater.* **2015**, *27*, 1432−1441.
(55) Shen, Y.; Roberge, A.; Tan, R.; Gee, M. Y.; Gary, D. C.; Huang, Y.; Blom, D. A.; Benicewicz, B. C.; Cossairt, B. M.; Greytak, A. B. Gel Permeation Chromatography as a Multifunctional Processor for Nanocrystal Purification and on-Column Ligand Exchange Chemistry. *Chem. Sci.* **2016**, *7*, 5671−5679.
(56) Roberge, A.; Stein, J. L.; Shen, Y.; Cossairt, B. M.; Greytak, A. B. Purification and in Situ Ligand Exchange of Metal-Carboxylate-Treated Fluorescent InP Quantum Dots Via Gel Permeation Chromatography. *J. Phys. Chem. Lett.* **2017**, *8*, 4055−4060.
(57) Park, N.; Monahan, M.; Ritchhart, A.; Friedfeld, M. R.; Cossairt, B. M. Synthesis of In37P20(O2CR)51 Clusters and Their Conversion to InP Quantum Dots. *JoVE* **2019**, *147*, No. e59425.

https://dx.doi.org/10.1021/acs.jpcc.0c09601
J. Phys. Chem. C 2021, 125, 2956−2965

(58) Miao, S.; Hickey, S. G.; Rellinghaus, B.; Waurisch, C.; Eychmüller, A. Synthesis and Characterization of Cadmium Phosphide Quantum Dots Emitting in the Visible Red to near-Infrared. *J. Am. Chem. Soc.* **2010**, *132*, 5613−5615.
(59) Zagdoun, A.; Rossini, A. J.; Gajan, D.; Bourdolle, A.; Ouari, O.; Rosay, M.; Maas, W. E.; Tordo, P.; Lelli, M.; Emsley, L.; et al. Non-Aqueous Solvents for DNP Surface Enhanced NMR Spectroscopy. *Chem. Commun.* **2012**, *48*, 654−656.
(60) Zagdoun, A.; Casano, G.; Ouari, O.; Schwarzwälder, M.; Rossini, A. J.; Aussenac, F.; Yulikov, M.; Jeschke, G.; Copéret, C.; Lesage, A.; et al. Large Molecular Weight Nitroxide Biradicals Providing Efficient Dynamic Nuclear Polarization at Temperatures up to 200 K. *J. Am. Chem. Soc.* **2013**, *135*, 12790−12797.
(61) Harris, R. K.; Becker, E. D.; Cabral de Menezes, S. M.; Goodfellow, R.; Granger, P. NMR Nomenclature. Nuclear Spin Properties and Conventions for Chemical Shifts - (IUPAC Recommendations 2001). *Pure Appl. Chem.* **2001**, *73*, 1795−1818.
(62) Dixon, W. T.; Schaefer, J.; Sefcik, M. D.; Stejskal, E. O.; Mckay, R. A. Total Suppression of Sidebands in CPMAS C-13 NMR. *J. Magn. Reson.* **1982**, *49*, 341−345.
(63) Trebosc, J.; Wiench, J. W.; Huh, S.; Lin, V. S.-Y.; Pruski, M. Studies of Organically Functionalized Mesoporous Silicas Using Heteronuclear Solid-State Correlation NMR Spectroscopy under Fast Magic Angle Spinning. *J. Am. Chem. Soc.* **2005**, *127*, 7587−7593.
(64) Gullion, T.; Schaefer, J. Rotational-Echo Double-Resonance NMR. *J. Magn. Reson.* **1989**, *81*, 196−200.
(65) Rossini, A. J.; Hanrahan, M. P.; Thuo, M. Rapid Acquisition of Wideline MAS Solid-State NMR Spectra with Fast MAS, Proton Detection, and Dipolar HMQC Pulse Sequences. *Phys. Chem. Chem. Phys.* **2016**, *18*, 25284−25295.
(66) Gan, Z. $^{13}C/^{14}N$ Heteronuclear Multiple-Quantum Correlation with Rotary Resonance and Redor Dipolar Recoupling. *J. Magn. Reson.* **2007**, *184*, 39−43.
(67) Fung, B. M.; Khitrin, A. K.; Ermolaev, K. An Improved Broadband Decoupling Sequence for Liquid Crystals and Solids. *J. Magn. Reson.* **2000**, *142*, 97−101.

https://dx.doi.org/10.1021/acs.jpcc.0c09601
J. Phys. Chem. C 2021, 125, 2956−2965